Polyhedron 102 (2015) 668–676

Contents lists available at ScienceDirect

Polyhedron

journal homepage: www.elsevier.com/locate/poly

Iron(III) salicylates of dipicolylamine bases showing photo-induced anticancer activity and cytosolic localization

Aditya Garai [a], Ila Pant [b], Paturu Kondaiah [b,*], Akhil R. Chakravarty [a,*]

[a] Department of Inorganic and Physical Chemistry, Indian Institute of Science, Sir C.V. Raman Avenue, Bangalore 560012, India
[b] Department of Molecular Reproduction and Development Genetics, Indian Institute of Science, Sir C.V. Raman Avenue, Bangalore 560012, India

ARTICLE INFO

Article history:
Received 20 August 2015
Accepted 17 October 2015
Available online 31 October 2015

Keywords:
Iron
Salicylic acid
Crystal structure
Photocytotoxicity
Cellular imaging

ABSTRACT

An iron(III) salicylate having a dipicolylamine base (andpa) with a photoactive anthracenyl moiety is prepared, characterized, and studied for its photo-induced anticancer activity and cellular localization in HeLa and MCF-7 cells. Its phenyl analogue is structurally characterized by X-ray crystallography. The complex has a ternary structure in which the dipicolylamine ligand and salicylic acid in dianionic form (sal) display respective tridentate and bidentate mode of coordination in [Fe(sal)(phdpa)Cl] (**1**). Complex [Fe(sal)(andpa)Cl] (**2**) having a pendant anthracenyl moiety shows significant photocytotoxicity in visible light (400–700 nm) giving IC_{50} values of 8.6 ± 0.7 and 3.4 ± 0.9 μM in HeLa and MCF-7 cells, while being essentially nontoxic in the dark (IC_{50} > 100 μM). The complex shows cytosolic localization in the cancer cells. Formation of hydroxyl radicals (·OH) as the reactive oxygen species is evidenced from the pUC19 DNA photocleavage studies.

1. Introduction

Iron–bleomycins (Fe–BLMs) as metalloglycopeptides are the naturally occurring anticancer antibiotics [1,2]. Their successful use in cancer therapy has led to the development of the chemistry of synthetic iron complexes as structural models and potent chemotherapeutic agents [3–8]. Iron–bleomycins act as chemical nucleases in which the metal in its high-spin +2 oxidation state activates molecular oxygen to form reactive hydroxyl species that oxidizes the deoxyribose sugar moiety causing damage to DNA [9]. There are only few synthetic models of iron–bleomycins reported in the literature using N-donor multidentate ligand systems stabilizing the metal in its +2 and +3 oxidation states [6–8]. Unlike the natural iron–bleomycins, these model complexes lack any selectivity towards cancer cells over normal cells. The currently available synthetic models are thus likely to damage the healthy cells due to their low IC_{50} values in the dark [6]. A convenient way to circumvent this predicament is to design iron complexes that are nontoxic in the dark under aerobic conditions but gains activity only when exposed to visible light of suitable wavelength. We have earlier shown that iron complexes could be suitably designed to show photo-induced anticancer activity [10–15]. Besides, complexes of other metal ions are also known to show photochemotherapeutic activity [16–25]. Six-coordinate platinum(IV) complexes having two trans-azide ligands are known to generate reactive platinum(II) species on photoactivation showing significant cytotoxicity even in cisplatin resistant cells [16]. Photocytotoxic nitrosyl ruthenium complexes are used to deliver toxic nitric oxide (NO) on exposure to visible light [17]. Dirhodium(II) complexes are reported to show cytotoxicity in visible light [18]. Copper(II) and oxovanadium(IV) complexes having photoactive moieties are known to show excellent PDT effect in visible light [19–22]. Photodynamic therapy (PDT) has evolved as a non-invasive treatment modality of cancer with promising results [23–25]. Porphyrin derivatives with the hematoporphyrin species Photofrin® is currently used as a PDT drug. With the advent of this new methodology, metal-based photochemotherapeutic agents have gained considerable importance as substitutes of the porphyrin-based PDT agents [26,27].

The present work stems from our interest to design new iron complexes which can show significant anticancer activity on photo-irradiation while remaining essentially inactive in the dark. We have chosen iron for being an essential metal for cellular growth including that for cancer cells [28]. The presence of large number iron receptors on cancer cells can be used to successfully transport iron-based anticancer agents into the cell [29]. Besides, there is no report on any major adverse impact of the metal in iron–bleomycins except pulmonary fibrosis [30]. A stable iron

* Corresponding authors. Tel.: +91 80 2293 3259; fax: +91 80 23600999 (P. Kondaiah). Tel.: +91 80 2293 2533; fax: +91 80 23600683 (A.R. Chakravarty).
E-mail addresses: paturu@mrdg.iisc.ernet.in (P. Kondaiah), arc@ipc.iisc.ernet.in (A.R. Chakravarty).

http://dx.doi.org/10.1016/j.poly.2015.10.026
0277-5387/

complex under physiological conditions can overcome the challenges associated with this metal. We have used dipicolylamine base having a pendant photoactive moiety for achieving the desired PDT activity. Salicylic acid in its dianionic form is used for its bio-essential nature and for its affinity to bind iron. Using these ligand systems we have been able to synthesize ternary complexes that show reduced chemical nuclease activity in the presence of reducing cellular thiols. The dipicolylamine base (andpa) having a pendant anthracenyl moiety as a fluorophore is used as a photosensitizer and to study cellular localization of the complex. Herein, we report the synthesis, crystal structure and visible light-induced cytotoxicity of two iron(III) salicylates, viz. [Fe(sal)(phdpa/andpa)Cl] (**1**, **2**), where phdpa is (phenyl)dipicolylamine (in **1**) and andpa is (anthracenyl)dipicolylamine (in **2**) (Fig. 1). Significant results of this study are the observation of remarkable PDT effect of the andpa complex **2** in visible light (400–700 nm) in cervical cancer HeLa and breast cancer MCF-7 cells along with cytosolic localization of the complex from the fluorescence microscopy.

2. Experimental

2.1. Materials and measurements

The chemicals and reagents were procured from the commercial sources (s.d. Fine Chemicals, India; Aldrich–Sigma, USA; Invitrogen Bio Services, India). They were used without further purification. Supercoiled plasmid pUC19 DNA (CsCl purified) was from Bangalore Genie (India). Tris-(hydroxymethyl)aminomethane–HCl (Tris–HCl) buffer was prepared using deionised and sonicated triple distilled water. Solvents used for this work were purified by standard procedures. Dipicolylamine bases, viz. *N*-benzyl-1-(pyridin-2-yl)-*N*-[(pyridin-2-yl)methyl]-methanamine (phdpa) and 1-(anthracen-9-yl)-*N*,*N*-bis(pyridin-2-ylmethyl)methanamine (andpa) were prepared following literature methods [31,32].

The elemental analyses were done with a Thermo Finnigan FLASH EA 1112 CHNS analyzer. The infrared, absorption and emission spectral measurements were done using Perkin-Elmer make model Lambda 35, Lambda 650 and LS 55 spectrophotometer, respectively, at 25 °C. Molar conductivity measurements were made using a Control Dynamics (India) conductivity meter. Electrochemical studies were done at 25 °C with an EG&G PAR model 253 VersaStat potentiostat/galvanostat with electrochemical analysis software 270 using a three-electrode setup that consists of a glassy carbon working, platinum wire auxiliary and a saturated calomel reference electrode (SCE). Tetrabutylammonium perchlorate (TBAP, 0.1 M) was used as a supporting electrolyte. ESI-MS measurements were made with a Bruker Daltonics make Esquire 300Plus ESI model. Flow cytometric analysis was performed using a FACS Verse (Becton Dickinson (BD)) cell analyzer at FL2 channel (595 nm). Fluorescence microscopy images were obtained from Zeiss LSM5 10 apochromat confocal laser scanning microscope. Magnetic measurements at 298 K were done using Sherwood Scientific, Cambridge (U.K.), magnetic susceptibility balance.

2.2. Preparation of [Fe(sal)(phdpa/andpa)Cl] (phdpa, *1*; andpa, *2*)

To a methanol solution of ferric chloride (0.16 g, 1.0 mmol) was added the dipicolylamine base (0.29 g phdpa for **1** and 0.39 g andpa for **2**, 1.0 mmol) dissolved in methanol (20 mL). The solution was stirred for 30 min to get a precipitate of the precursor complex [Fe (phdpa/andpa)Cl_3] to which was added drop-wise a solution of salicylic acid (H_2sal, 0.14 g, 1.0 mmol) and triethylamine (0.10 g, 1.0 mmol) in 10 mL methanol to obtain a deep purple colored solution which on slow evaporation of the solvent gave a solid that was isolated, washed with diethyl ether and finally dried in vacuum over P_4O_{10}.

*[Fe(sal)(phdpa)Cl] (**1**):* Yield: 0.42 g (75%). *Anal.* Calc. for $C_{26}H_{23}ClFeN_3O_3$ (MW: 516.78): C, 60.43; H, 4.49; N, 8.13. Found: C, 60.69; H, 4.27; N, 7.80. ESI-MS in MeOH: *m*/*z* 481.1038 $[M - Cl^-]^+$. IR (in solid phase, cm^{-1}): 2940 (m), 2650 (m), 2370 (m), 1600 (s), 1500 (s), 1390 (s), 1280 (m), 1150 (s), 1030 (s), 975 (s), 815 (w), 770 (m), 730 (m), 550 (w), 450 (m) cm^{-1} (s, strong; m, medium; w, weak). UV–Vis (DMF) λ_{max}, nm (ε, M^{-1} cm^{-1}) = 450 (1300), 290 (3360). Molar conductance in DMF at 25 °C: Λ_M = 69 S m^2 M^{-1}. μ_{eff} = 5.85 μ_B at 298 K.

*[Fe(sal)(andpa)Cl] (**2**):* Yield: 0.54 g (79%). *Anal.* Calc. for $C_{34}H_{27}ClFeN_3O_3$ (MW: 616.90): C 66.20, H 4.41, N 6.81. Found: C 65.50, H 4.67, N 6.61. ESI-MS in MeOH: *m*/*z* = 580.99 $[M - Cl^-]^+$. IR (in solid phase, cm^{-1}): 2950 (br), 2600 (m), 2490 (m), 2350 (s), 1660 (m), 1580 (s), 1450 (s), 1360 (m),1270 (m), 1230 (m), 1150 (m), 1000 (m), 815 (s), 750 (s), 650 (s), 570 (w), 530 (w), 470 (w), 430 (w) cm^{-1} (br, broad). UV–Vis (DMF) λ_{max}, nm (ε, M^{-1} cm^{-1}): 450 (1256), 390 (4450), 370 (4470), 350 (3200), 333 (2440), 300 (5350). Molar conductance in DMF at 25 °C: Λ_M = 72 S m^2 M^{-1}. μ_{eff} = 5.80 μ_B at 298 K.

2.3. X-ray crystallographic procedure

The crystal structure of [Fe(sal)(phdpa)Cl] H_2O was obtained by X-ray diffraction method. Crystals of **1** as a monohydrate were obtained from a methanol solution of the complex on slow evaporation of the solvent. A suitable crystal was mounted on a glass fiber with epoxy cement and the geometric and intensity data were collected at room temperature using an automated Bruker SMART APEX CCD diffractometer equipped with a fine-focus 1.75 kW sealed-tube Mo Kα X-ray source (λ = 0.71073 Å) with increasing ω (width of 0.3° per frame) at a scan speed of 5 s per frame. Intensity data were collected using ω-2θ scan mode and corrected for Lorentz-polarization effects and for absorption [33]. The structure solution was done by a combination of Patterson and Fourier techniques and full-matrix least-squares refinement was done using

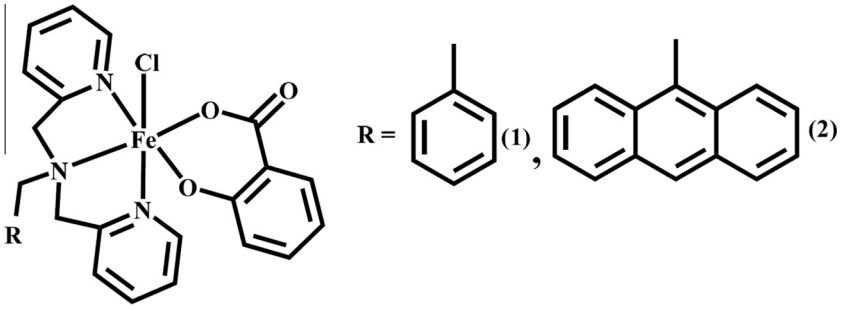

Fig. 1. Schematic drawings of the complexes **1** and **2**.

SHELX system of programs [34]. Hydrogen atoms of the complex that were placed in their calculated positions were refined using a riding model. Positional disorder of few atoms of the dianionic salicylate ligand was observed during the structure solution and refinement. The concerned atoms in two groups, viz. labeled-A and labeled-B, were refined with a site occupancy of 0.5. The disorder treatment was done using the provisions available in the SHELX program. The salicylate aromatic ring carbon atoms C30, C31 and C32 and the non-coordinated oxygen atom O(3) were found to have positional disorder and they were grouped to two parts [A and B] each corresponding to one set. This disorder did not have any apparent effect on the chemistry of the complex. The non-hydrogen atoms bearing the disordered ones were refined anisotropically. The molecular view was obtained by using ORTEP [35].

2.4. Cellular experiments

MTT assay was done to assess the photocytotoxicity of the complexes [36]. Details of the experimental procedures are given as Supplementary information. Photo-irradiation of the cells was done in visible light of 400–700 nm using a Luzchem photoreactor (model LZC-1, Ontario, Canada; light fluence rate = 2.4 mW cm^{-2}; light dose = 10 J cm^{-2}). Molecular Devices Spectra Max M5 plate reader was used for measuring the absorbance of formazan at 540 nm. The cytotoxicity of the test compounds was measured as the percentage ratio of the absorbance of the treated cells over the untreated controls. The IC_{50} values were determined by nonlinear regression analysis (GraphPad Prism 5). Flow cytometric analysis was performed to study the rate of uptake of complex **2** into HeLa and MCF-7 cancer cells and effect on the cell cycle by complex **2**. Detailed procedure is given in Supporting information. DCFDA and annexin-V/FITC assays were used to detect generation of cellular reactive oxygen species (ROS) and apoptotic process by flow cytometric analysis [37]. Cell permeable DCFDA on oxidation by ROS generates fluorescent DCF having an emission maximum at 528 nm. The distribution of DCFDA stained HeLa cells was determined by flow cytometry. Annexin-V/FITC assay was used to study the apoptotic cell death. Detailed procedures are given as Supplementary information. The fluorescence of the cells was determined with a flow cytometer. Cells involved in the early apoptotic process were stained with the annexin V-FITC alone. Live cells showed no staining by either propidium iodide or annexin V-FITC and necrotic cells were stained by both propidium iodide and annexin V-FITC. Fluorescence microscopy was used to study uptake of the fluorescent complex **2** into the HeLa cells using a procedure that is given as Supplementary material.

2.5. DNA binding and cleavage experiments

DNA binding experiments were done in Tris–HCl buffer (5 mM, pH = 7.2) using DMF solution of the complexes **1** and **2** using reported procedures [12]. Calf thymus DNA (ca. 250 μM NP) was used for the binding studies. The intrinsic equilibrium binding constant (K_b) of **1** and **2** to ct-DNA were obtained by the McGhee–von Hippel (MvH) method using the expression of Bard et al. by monitoring the change of the absorption intensity of the spectral band with increasing concentration of ct-DNA [38,39]. The viscosity measurements were done using a Schott Gerate AVS 310 automated viscometer attached to a constant temperature bath at 37 °C. DNA thermal denaturation studies were done by monitoring the absorption intensity of ct-DNA (150 μM) at 260 nm using UV-2600 Shimadzu model CPS-240A and Peltier CPS-240 A spectrometer with a controller at an increase rate of 1 °C min^{-1} of the solution. The cleavage of SC pUC19 DNA (0.2 μg, 30 μM, 2686 base-pairs) was studied by agarose gel electrophoresis using the complexes in 50 mM Tris–HCl buffer (pH 7.2) and 50 mM NaCl containing 10% DMF in light of 532 nm using Ar–Kr mixed gas ion laser of Spectra Physics with a laser power 100 mW using a reported procedure [12]. Mechanistic studies were carried out using different additives. The extent of SC DNA cleavage was measured from the intensities of the bands using the UVITEC Gel Documentation System. The observed error in measuring the band intensities was ca. 5%.

3. Results and discussion

3.1. Synthesis and general aspects

The iron(III) salicylates [Fe(sal)(phdpa/andpa)Cl] (**1**, **2**) were prepared by reacting a methanol solution of the dipicolylamine derivative with $FeCl_3$ to obtain a precursor complex which on further treatment with salicylic acid (H_2sal) and triethylamine in methanol formed the complexes in high yield. The complexes were characterized from the analytical, spectral and other physicochemical data (Table 1). The ESI-MS of the complexes in methanol displayed a prominent peak corresponding to the $[M - Cl^-]^+$ species. The complexes are found to be 1:1 electrolyte in DMF giving a molar conductivity (Λ_M) value of ~70 S m^2 M^{-1} due to dissociation of the chloride ligand as evidenced from the ESI-MS spectra. The electronic absorption spectra of the complexes in DMF showed a broad but intense peak near 450 nm with a tail extending up to 600 nm (Fig. 2). The spectral peaks in the UV region are assignable to the π–π^* transitions involving the ligands [40]. The low energy visible band is assignable to the ligand-to-metal charge transfer (LMCT) transition as observed for an analogous hydroxamate complex [12]. Complex **2** showed an emission band at 420 nm upon excitation at 370 nm giving a quantum yield (φ) value of 0.04 in DMSO (Fig. 2). The φ value of the andpa ligand is 0.13 under similar experimental conditions. The IR spectra of the complexes displayed a strong peak at 1600 cm^{-1} corresponding to the C=O stretching vibrations of the salicylate ligand [41]. The iron(III) complexes are paramagnetic with five unpaired electrons giving room temperature magnetic moment value of ~5.75 μ_B. Cyclic voltammetry of the complexes showed a quasi-reversible Fe(III)–Fe(II) redox couple with an $E_{1/2}$ value of ~0.05 V versus SCE in DMF-0.1 M TBAP with large ΔE_p value indicating sluggish electron transfer process with the possibility of a structural change on reduction of the metal (Fig. 3(a)). The presence of E_{pc} near −0.5 V indicates the redox stability of +3 oxidation state of the metal. This is likely to

Table 1
Selected physicochemical and ct-DNA binding data of the complexes **1** and **2**.

	1	**2**
IR[a]/cm^{-1}[$\bar{\nu}$ (C=O)]	1600	1580
Electronic[b]: λ_{max}/nm (ε/M^{-1} cm^{-1})	450 (1300)	466 (1250)
Emission[c] [λ_{em}/nm] (φ)	–	420 (0.04)
μ_{eff}[d]	5.85	5.80
Λ_M[e]/S m^2 M^{-1}	69	72
E_f[f]/$V(\Delta E_p$/mV)	0.071 (640)	0.067 (650)
K_b[g]/M^{-1}	$(2.2 \pm 0.5) \times 10^5$	$(4.4 \pm 0.8) \times 10^5$
ΔT_m[h]/°C	1	3

[a] In KBr phase.
[b] Visible electronic spectral band in DMF.
[c] Emission peak of **2** in DMSO with λ_{ex} of 370 nm φ, the quantum yield value.
[d] Magnetic moment (μ_{eff}) in μ_B.
[e] Λ_M, molar conductance in DMF at 25 °C.
[f] Fe(III)–Fe(II) redox couple in DMF/0.1 M TBAP at 50 mV s^{-1} scan rate.
[g] Equilibrium DNA binding constant determined from the UV–visible absorption titration.
[h] DNA melting temperature.

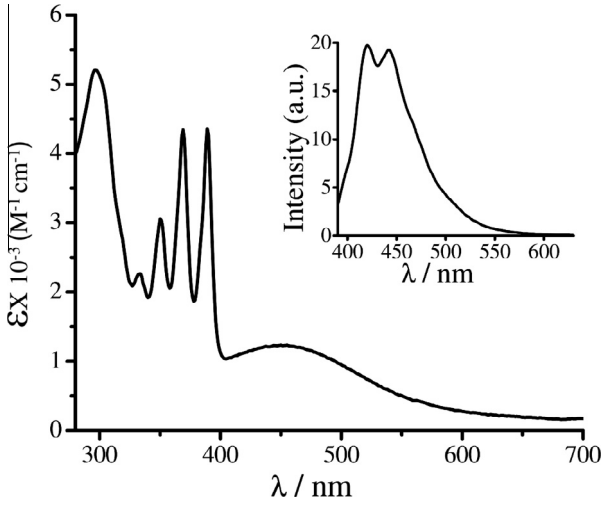

Fig. 2. UV–Visible spectrum of complex **2** in DMF with the inset showing its emission spectrum in DMSO (λ_{ex} = 370 nm).

reduce the chemical nuclease activity of the complexes in presence of reducing agents. Addition of 3-mercaptopropionic acid to the solution of complex **2** showed gradual decrease in the UV–visible spectral peak absorbance of the LMCT band (Fig. 3(b)). This could be due to reduction of the metal to its +2 oxidation state [42].

3.2. Crystal structure

Complex **1**, as its monohydrate, was structurally characterized by single-crystal X-ray crystallography. It crystallized in $P2_1/n$ space group of the monoclinic crystal system. Selected crystallographic data and important bond distance and bond angle parameters are given in Tables 2 and 3, respectively. The structure shows the iron in a six coordinate $\{Fe^{III}N_3O_2Cl\}$ geometry in which the metal is bonded to the tridentate *N,N,N*-donor (phenyl)dipicolylamine ligand in a facial mode of bonding, bidentate *O,O*-donor salicylate dianion and a chloride ligand. The coordination geometry is significantly distorted from an octahedral structure. During structure solution, few atoms of the salicylate ligand were found to have positional disorders. This disorder, however, had no impact on the overall structure of this complex. The disordered atoms were refined with same site-occupancy and were labeled as (A) and (B). The ORTEP diagram of the complex in Fig. 4 shows both orientations of the salicylate ligand. The Fe(1)–N(2) bond with the N(2) atom in a sp^3 hybridization is found to be longer than the other two Fe–N distances. The Fe–O distances are ~2.0 Å. The Fe–Cl bond

Table 2
Selected crystallographic data for [Fe(sal)(phdpa)Cl] H_2O (**1** H_2O).

Empirical formula	$C_{26}H_{23}ClFeN_3O_3$
Formula weight (g M^{-1})	516.77
Crystal system	monoclinic
Space group	$P2_1/n$
a (Å)	10.2616(9)
b (Å)	15.6897(9)
c (Å)	15.6060(15)
$\alpha = \gamma$ (°)	90.0
β (°)	106.379(10)
V (Å^3)	2410.6(4)
Z	4
T (K)	293 (2)
ρ_{calc} (g cm^{-3})	1.424
λ (Å) (Mo Kα)	0.71073
μ (cm^{-1})	0.770
Data/restraints/parameters	6533/0/333
F (000)	1068
Goodness-of-fit (GOF)	1.048
$R(F_o)$[a], $I > 2\sigma(I)$[wR (F_o)][b]	0.0804[0.1879]
R (all data) [wR(all data)]	0.1424 [0.2253]
Largest diff. peak and hole (e Å^{-3})	0.896, −0.301

[a] $R = \Sigma||F_o| - |F_c||/\Sigma|F_o|$.
[b] $wR = \Sigma[w(F_o^2 - F_c^2)^2]/\Sigma[w(F_o)^2]\}^{1/2}$. $w = [\sigma^2F_o^2+(AP)^2 + BP]^{-1}$, where $P = (F_o^2 + 2F_c^2)/3$, $A = 0.0433$; $B = 0.7893$.

Table 3
Selected bond distances (Å) and bond angles (°) for [Fe(sal)(phdpa)Cl] H_2O (**1** H_2O).

Fe(1)–O(1)	1.907(3)	O(2)–Fe(1)–N(2)	99.27(13)
Fe(1)–O(2)	1.920(3)	O(2)–Fe(1)–N(3)	85.39(15)
Fe(1)–N(1)	2.194(3)	O(1)–Fe(1)–Cl(1)	102.60(11)
Fe(1)–N(2)	2.271(4)	O(2)–Fe(1)–Cl(1)	95.98(11)
Fe(1)–N(3)	2.146(4)	N(1)–Fe(1)–N(2)	73.61(13)
Fe(1)–Cl(1)	2.3135(14)	N(1)–Fe(1)–N(3)	94.28(15)
O(1)–Fe(1)–O(2)	90.09(14)	N(2)–Fe(1)–N(3)	76.14(17)
O(1)–Fe(1)–N(1)	87.83(14)	N(1)–Fe(1)–Cl(1)	91.30(10)
O(1)–Fe(1)–N(2)	86.00(15)	N(2)–Fe(1)–Cl(1)	162.48(10)
O(1)–Fe(1)–N(3)	160.58(16)	N(3)–Fe(1)–Cl(1)	96.66(13)
O(2)–Fe(1)–N(1)	172.70(14)		

distance is 2.313(8) Å. The N(1)–Fe(1)–N(3) bond angle is 94.28 (16)°. The O(1)–Fe(1)–O(2) angle is 90.03(14)°. The crystal structure is found to get stabilized by non-covalent π–π interaction involving two pyridyl rings at a distance of 3.8 Å between two centroids of the rings. Complex **1** shows different bonding features compared to its benzhydroxamate analogue [12]. The Fe–Cl bond in the benzhydroxamate complex is trans to the Fe–O bond, while complex **1** has the Fe–Cl bond trans to the Fe(1)–N(2) bond. The

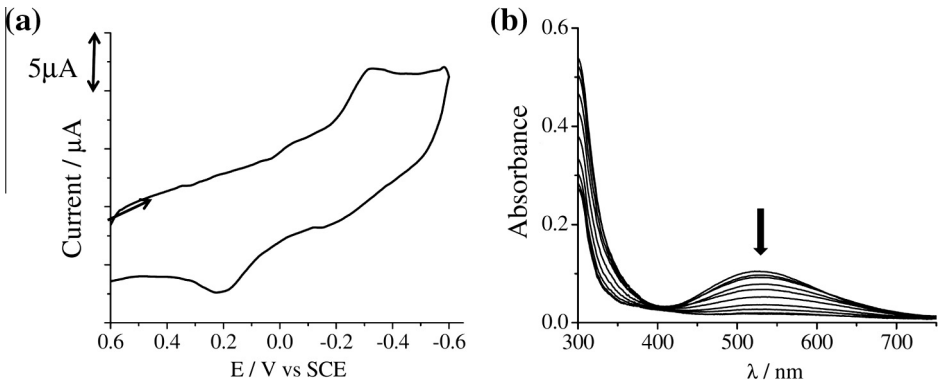

Fig. 3. (a) Cyclic voltammogram of complex **2** showing quasi-reversible Fe(III)–Fe(II) redox couple in DMF–0.1 M TBAP. (b) Addition of 3-mercaptopropionic acid to the solution of complex **2** showing a gradual decrease in the UV–visible spectral peak absorbance.

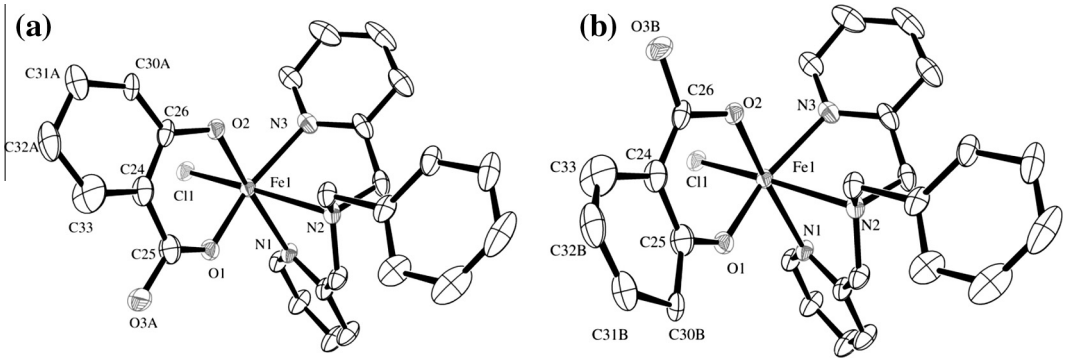

Fig. 4. An ORTEP view of [Fe(sal)(phdpa)Cl] (**1**) showing atom numbering scheme for the metal and hetero-atoms. The hydrogen atoms are omitted for clarity. The positional disordered arrangements (1:1) are shown by labeling A and B.

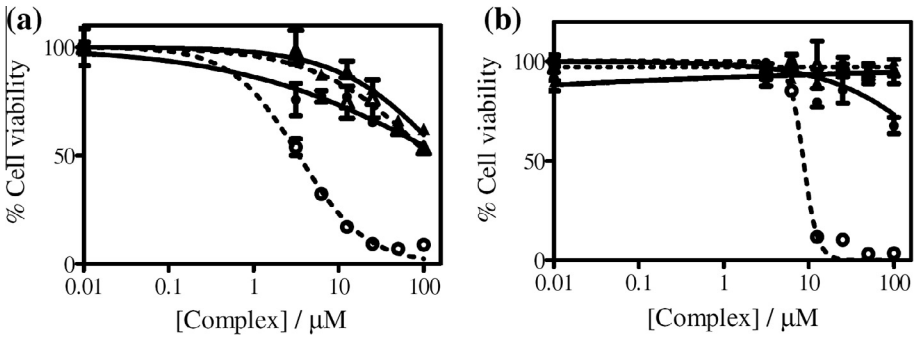

Fig. 5. (a) Photocytotoxicity of complexes **1** and **2** in HeLa cancer cells on 4 h incubation in the dark (black circle and solid line) and after irradiation with visible light of 400–700 nm (10 J cm^{-2}, open circle and dash line). (b) Photocytotoxicity of complexes **1** and **2** in MCF-7cancer cells on 4 h incubation in the dark (black circle and solid line) and after irradiation with visible light of 400–700 nm (10 J cm^{-2}, open circle dash line).

Table 4
IC_{50} values of **1**, **2** and related compounds in HeLa cancer cells.

Complex	IC_{50} (μM) in light (400–700 nm)	IC_{50} (μM) in the dark
1[a]	>100	>100
2[a]	8.6 ± 0.7	>100
$[Fe(phqpy)]^{2+}$[b]	–	7.7 ± 0.1
Photofrin[c]	4.3 ± 0.2	>41
Cisplatin[d]	–	20.5 ± 0.2
[FeL′(cat)NO_3][f]	6.2 ± 0.1	>100
[Fe(BHA)(pydpa)Cl]Cl[g]	14.6 ± 0.7	77.0

[a] The IC_{50} in light is on visible light irradiation (400–700 nm, 10 J cm^{-2}). The values are >100 μM for **1** and 3.4 ± 0.9 μM for **2** in MCF-7 cells in light (400–700 nm). The complexes are inactive in darkness in MCF-7 cancer cells.
[b] Value taken from Ref. [6]. Ligand phqpy is 2,2′:6′, 2″:6″,2‴:6‴,2⁗-phenylquinquepyridine.
[c] Values taken from Ref. [43].
[d] Value taken from Ref. [6].
[f] Ref. [10]. L′ is 1-(anthracen-9-yl)-*N*,*N*-bis(pyridin-2-ylmethyl)methanamine.
[g] Reference [12]. BHA is benzhydroxamate anion. Ligand pydpa is (pyrenyl) dipicolylamine.

hydroxamate and salicylate iron(III) complexes thus differ in their molecular structures.

3.3. Solubility and stability

The complexes were soluble in common organic solvents like methanol, ethanol, DMF, DMSO, acetonitrile with moderate solubility in water. They were, however, insoluble in hydrocarbon solvents. The solution stability of the complexes was studied by UV–visible spectroscopy in aqueous DMSO (1:1 v/v). There was no spectral change observed even after 48 h. This suggests that the complexes are stable in an aqueous medium thus making them suitable for cellular studies.

3.4. Cellular studies

MTT assay was done to assess the cytotoxicity of the complexes in visible light (400–700 nm, Luzchem photoreactor, light dose of 10 J cm^{-2}) in human cervical HeLa cancer cells and breast cancer MCF-7 cells. The complexes were found to be essentially non-toxic in the dark giving IC_{50} values of >100 μM. Complex **2**, however, showed significant photo-induced cytotoxicity in visible light of 400–700 nm with IC_{50} values of 8.6 ± 0.7 and 3.4 ± 0.9 μM in HeLa and MCF-7 cells, respectively (Fig. 5). The control complex **1** which lacks any photoactive moiety did not show any significant photocytotoxicity. The andpa ligand was inactive with an IC_{50} value of >100 μM in light. A comparison of the IC_{50} values of the present and related complexes is made in Table 4 [6,12,43].

Cellular uptake of complex **2** was studied for 2 and 4 h incubation in MCF 7 and HeLa cells (Fig. 6). After 2 h incubation the uptake of the complex in HeLa cells was found to be ~77% whereas in MCF-7 cell line it was ~95%. Even after 4 h of incubation the uptake in HeLa was ~85% whereas that of MCF-7 cells was ~96%. Therefore, complex **2** displayed better uptake in MCF-7 cells as compared to HeLa. To investigate the role of complex **2** in cell cycle progression, the DNA content of the cells treated with complex **2** was measured using propidium iodide (PI) in a fluorocytometer. The experiments were carried out in light as well as in darkness. Complex **2** in the dark did not show any significant cell death (Sub G1 population) but upon light irradiation it showed sub G1

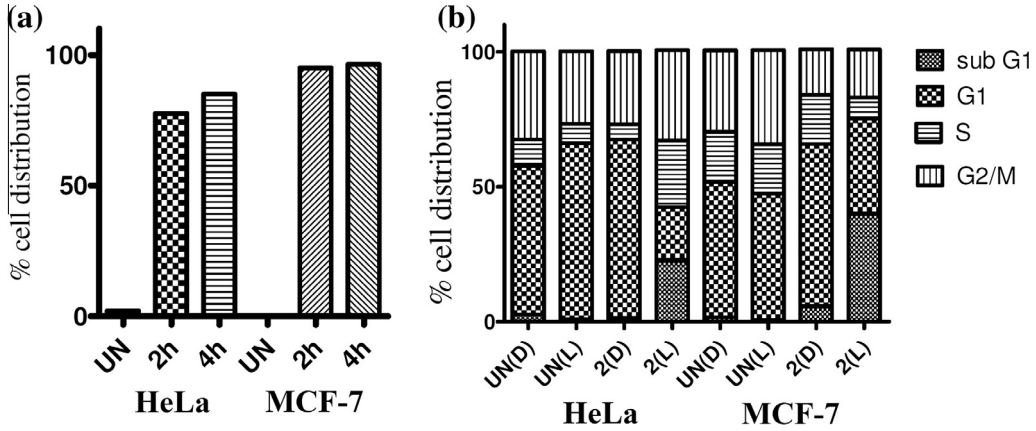

Fig. 6. (a) FACS study for the uptake of the complex **2** in HeLa and MCF-7 cell lines. (b) Bar diagram showing cell cycle distribution (sub-G1, G1, S, and G2/M phases) of the HeLa and MCF-7 cells treated with complex **2** and irradiated with visible light of 400–700 nm (10 J cm^{-2}), along with the dark controls.

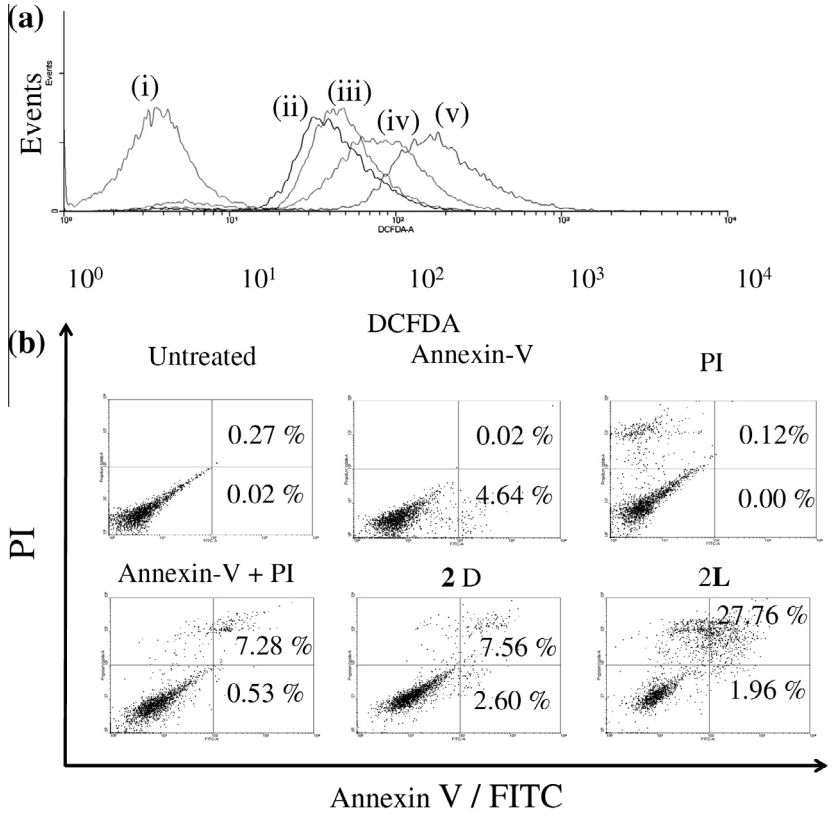

Fig. 7. (a) The shift in the fluorescence band position compared to the untreated cells in DCFDA assay measured by FACS analysis: (i) only cells, (ii) cells + DCFDA, (iii) cells + DCFDA + complex **2** (in the dark), (iv) cells + DCFDA + complex **2** (on light activation) and (v) cells + DCFDA + H_2O_2. (b) Cells treated with propidium iodide (PI), annexin-V/FITC conjugate and the complex. The data in the panels are for the% of healthy cells (LL), early apoptotic cells (LR), late apoptotic cells (UR) and necrotic cells (UL) in the different quadrants.

population of 22% and 40% in HeLa and MCF-7 cells respectively. This is in accordance with the MTT assay data wherein MCF7 cells (breast cancer cell line) were observed to be more sensitive to complex **2** mediating phototoxicity than the HeLa cells.

The mechanistic aspects of the cell death in HeLa cells was studied from the 2′,7′-dichlorodihydrofluorescein diacetate (DCFDA) assay (Fig. 7(a)). DCFDA is a cell permeable fluorogenic probe. This dye on oxidation by ROS forms 2′,7′-dichlorofluorescein (DCF) giving an emission maximum at 528 nm. The detection of DCF fluorescence and quantification from the fluorescence-activated cell sorting (FACS) analysis gave the evidence of ROS generation. HeLa cells were treated with complex **2** (20 μM) and DCFDA. The cells kept in dark did not show any enhancement in green fluorescence upon treatment with complex **2**. However, when they were exposed to visible light (400–700 nm), a significant shift in green fluorescence was observed indicating ROS generation. The annexin V-FITC/PI assay was performed with HeLa cells to explore if the cell death is via apoptotic pathway. Propidium iodide (PI) emits in the red region. The annexin V-FITC dye showed green fluorescence. This methodology allowed us for quantification of the apoptotic cells (early – annexin high, PI low; late – annexin and PI high), viable cell (unstained, only showing auto-fluorescence) and dead

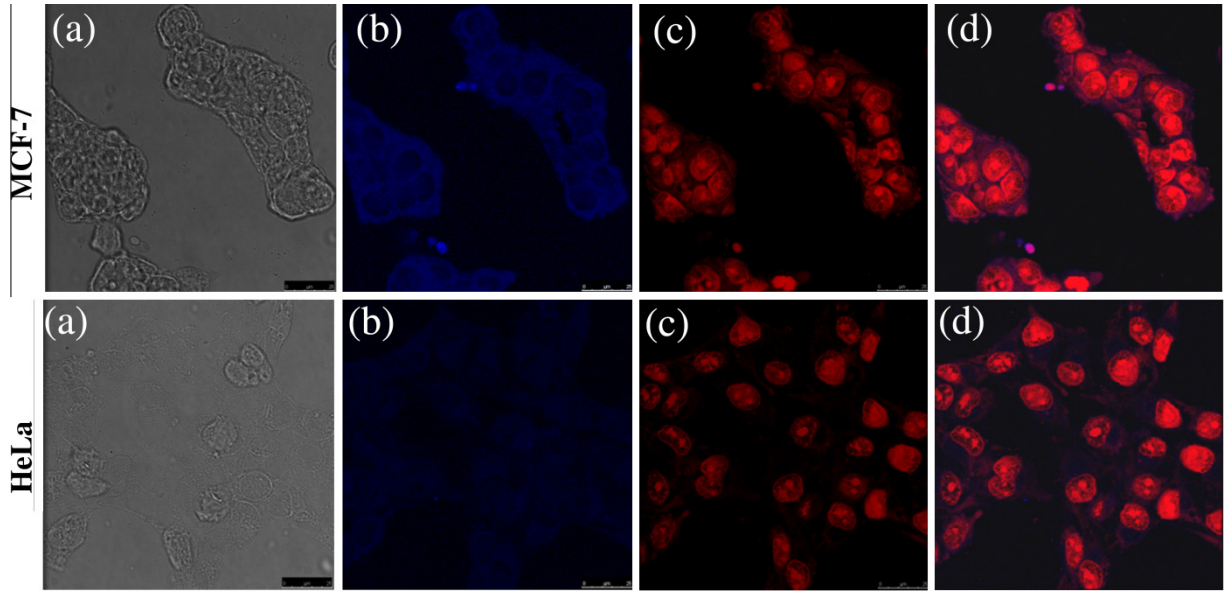

Fig. 8. Fluorescence microscopy images of complex **2** in MCF-7 and HeLa cells recorded after 4 h incubation using propidium iodide (PI): panels (a) bright field image (differential interference contrast); (b) correspond to fluorescence of complex **2**; panels (c) correspond to PI and panel (d) correspond to the merge images. Scale bar corresponds to 0.8 μm.

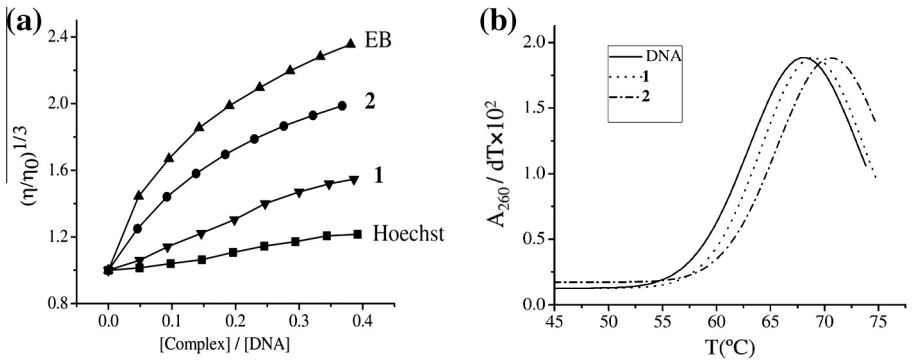

Fig. 9. (a) Plots showing the effect of addition of an increasing quantity of **1** or **2**, ethidium bromide (EB) and Hoechst dye on the relative viscosity of ct-DNA (150 μM) at 37.0 °C (EB, ethidium bromide). (b) DNA melting plot showing the increase in the DNA melting temperature upon binding to complexes giving ΔT_m value 1 and 3 for **1** and **2** respectively.

cell populations (stained by PI). The complex had apoptosis inducing potential as evidenced from the dot plots shown in Fig. 7(b). The percentage population of the viable cells decreased while that in the fourth quadrant Q3 and Q4 showed an increase, indicating that complex **2** triggered apoptosis only on light exposure. Complex **2** having a pendant anthracene moiety showing fluorescence was used to study the cellular uptake and localization of this complex in the cancer cells. The cells were incubated with complex **2** in the dark for 4 h. A significant uptake of the complex in the cytosol was evidenced from the fluorescence microscopy images along with that of nuclear staining dye propidium iodide (PI) (Fig. 8). The complex was found to be retained in the cytosol even after 4 h of incubation.

3.5. Binding and photo-cleavage of DNA

The binding propensity of the complexes to calf-thymus (ct) DNA was studied by UV–visible titration and viscometric methods. The equilibrium ct-DNA binding constant (K_b) values of the complexes were obtained from the UV–visible absorption experiments by monitoring the change in the absorption intensity of the ligand-centred band of the complexes near 370 nm for **2** and 270 nm for **1**. A significant hypochromicity along with minor bathochromic shift of the band suggests groove binding nature of the complexes to ct-DNA. The K_b values of 2.2×10^5 and 4.4×10^5 M^{-1} for **1** and **2** indicate good DNA binding strengths of the complexes. The relative specific viscosity of ct-DNA on binding to the complexes was obtained from viscometric titration experiments. The relative specific viscosity (η/η_0) of DNA gave a measure of the increase in the contour length associated with the separation of DNA base pairs caused by intercalation of the complex between DNA base pairs (η and η_0 are the specific viscosities of DNA in the presence and absence of the complex respectively). A DNA intercalator like ethidium bromide (EB) showed significant increase in viscosity of the ct-DNA solution. In contrast, the groove or surface binding dye induced only minor changes in the effective length of DNA resulting smaller changes in the relative viscosity of the ct-DNA solution. The viscometric titration plot of $(\eta/\eta_0)^{1/3}$ versus [complex]/[ct-DNA] ratio indicated partial intercalative mode of binding of complex **2** to ct-DNA (Fig. 9(a)). The DNA binding nature of the complexes to ct-DNA was studied from DNA denaturation experiments in a phosphate buffer of pH 6.8. The observed small

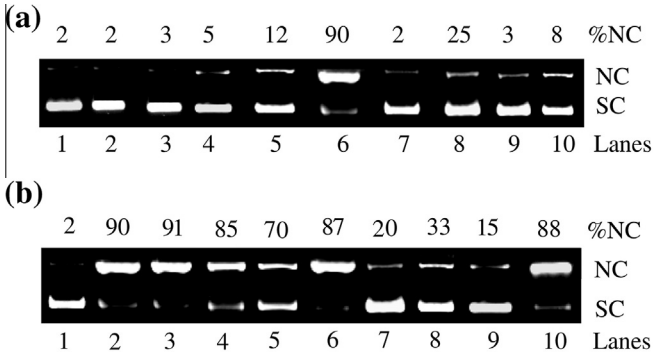

Fig. 10. (a) Gel diagram showing the cleavage of SC pUC19 DNA (0.2 μg, 30 μM) by [Fe(sal)(phdpa/andpa)Cl] (50 μM, L = phdpa, **1**; andpa, **2**) and ligands in 50 mM Tris–HCl/NaCl buffer (pH = 7.2) containing 10% DMF on addition of reducing agent in dark (lanes 7–10) and on irradiation with light of 532 nm (2 h exposure) (lanes 1–6) with controls: lane 1, DNA control; lane 2, DNA + $FeCl_3$; lane 3, DNA + phdpa; lane 4, DNA + andpa; lane 5, DNA + **1**; lane 6, DNA + **2**; lane 7, DNA + MPA; lane 8, DNA + MPA + 2; lane 9, DNA + H_2O_2; lane 10, DNA + H_2O_2 + **2**. (b) The gel diagram showing the photocleavage of pUC19 DNA in the presence of different additives. The lanes are: lane1, DNA control; lane 2, DNA + **2**; lane 3, DNA + **2** + DABCO (0.5 mM); lane 4, DNA + **2** + TEMP (0.5 mM); Lane 5, DNA + **2** + NaN_3 (0.5 mM); lane 6, DNA + **2** + L-Histidine (0.5 mM); lane 7, DNA + **2** + DMSO (0.5 mM); lane 8, DNA + **2** + KI (0.5 mM); lane 9, DNA + **2** + catalase (4 units); lane 10, DNA + **2** + SOD (5 units).

shift in the DNA melting temperature suggests groove binding nature of the complexes when compared to that of ethidium bromide that gave a large value of ΔT_m which is well known as DNA intercalator (Fig. 9(b)).

The chemical nuclease activity of the complexes was studied in the presence of hydrogen peroxide (H_2O_2, 200 μM) as an oxidizing agent and 3-mercaptopropionic acid (MPA, 1.0 mM) as a reducing agent using supercoiled (SC) pUC19 DNA (0.2 μg, 30 μM) in 50 mM Tris–HCl/50 mM NaCl buffer (pH 7.2). The extent of DNA cleavage was estimated from the gel electrophoresis data shown in Fig. 10(a). The iron(III) complexes showed only moderate chemical nuclease activity in the presence of MPA due to less possibility of the formation of the reactive iron(II) species in the presence of high negative E_{pc} value of ca. −0.5 V versus SCE. Iron(II) species formed due to one-electron reduction of iron(III) complex can readily generate hydroxyl radicals by activating molecular oxygen as is known for the activity of iron–bleomycins [9]. Control experiments using the dipicolylamine ligand, salicylic acid, H_2O_2 and MPA alone did not show any apparent cleavage of DNA under similar experimental conditions. The photo-induced DNA cleavage activity of the complexes was studied using green light of 532 nm from a CW Ar–Kr mixed gas ion laser and the gel diagram is shown in Fig. 10(a) along with the controls. Complex **2** is an efficient photocleaver of SC DNA. A 50 μM solution of this complex showed essentially complete cleavage of the SC DNA to its nicked circular (NC) form upon irradiation with green light of 532 nm for 2 h. The complexes did not show any DNA cleavage activity in the dark. Control experiments with the metal salt or the ligands alone showed no apparent photocleavage of DNA. The complexes bind to the major groove of DNA. Addition of DNA minor groove blocker distamycin did not inhibit the DNA cleavage activity. Addition of methyl green as the DNA major groove blocker significantly reduced the cleavage activity of the complexes.

The mechanistic aspects of the DNA photocleavage reactions were studied using different additives, viz. 1,4-diazabicyclo[2.2.2] octane (DABCO, 1.0 mM), 2,2,6,6-tetramethylpiperidine (TEMP, 1.0 mM), sodium azide (NaN_3, 1.0 mM) and L-histidine (1.0 mM) as singlet oxygen quenchers and DMSO (4 μL), KI (1.0 mM) and catalase (4 units) as hydroxyl radical scavengers, and superoxide dismutase (SOD, 4 units) as superoxide radical scavenger. The gel diagram is shown in Fig. 10(b). The hydroxyl radical scavengers showed significant inhibition, while singlet oxygen quenchers showed no apparent effect on the DNA cleavage activity. The photo-induced DNA cleavage activity involving the absorption band in the visible region may follow a metal-assisted mechanistic pathway forming the hydroxyl radicals. The photo-redox pathway is a possibility in which reduction of Fe(III) on photo-activation could form a charge separated Fe^{2+}–$L^{\cdot+}$ (ligand radical cation) species that reduces O_2 to $O_2^{\cdot-}$ by the reactive Fe^{2+} ion with subsequent formation of hydroxyl radicals ($HO^{\cdot}$) in the reaction: $3O_2^{\cdot-} + 2H^+ \rightarrow HO^{\cdot} + HO^- + 2O_2$ [4]. This pathway is facilitated in the presence of a quasi-reversible Fe(III)–Fe(II) redox couple. The ROS involved in the cellular damage could be reactive hydroxyl species as evidenced from the plasmid DNA photocleavage study (see Fig. 10).

4. Conclusions

The iron(III) salicylate of a dipicolylamine base with a pendant photoactive anthracenyl moiety shows remarkable PDT effect with an IC_{50} value of ~3 and ~8 μM in MCF-7 and HeLa cancer cells while being essentially non-toxic in the dark. The complex also shows cytosolic localization with the possibility of mitochondrial DNA being the target. The complexes show excellent ct-DNA binding strengths. Photocleavage of plasmid DNA involves formation of hydroxyl radicals. The iron centre in a ternary structure plays an important role as the ligands alone are inactive. A Fenton-type mechanism seems to be operative in a similar way as is known for iron–bleomycins. The complexes show only moderate chemical nuclease activity when compared to the iron-based model complexes of bleomycins. The results are of significance considering that the iron-based anticancer agents showing cytosolic localization and remarkable PDT activity in visible light (400–700 nm) are potentially suitable for photo-chemotherapeutic applications.

Acknowledgements

A.R.C. is thankful to the Department of Science and Technology (DST), Government of India, for funding (SR/S5/MBD-02/2007) and for J.C. Bose National fellowship. Thanks are due to the Alexander von Humboldt Foundation (Germany) for donation of an electrochemical system and DST for a CCD diffractometer facility. We thank D.K. Swain for his help in solving the crystal structure.

Appendix A. Supplementary data

CCDC 1407971 contains the supplementary crystallographic data for this paper. These data can be obtained free of charge via http://www.ccdc.cam.ac.uk/conts/retrieving.html, or from the Cambridge Crystallographic Data Centre, 12 Union Road, Cambridge CB2 1EZ, UK; fax: (+44) 1223 336 033; or e-mail: deposit@ccdc.cam.ac.uk. Supplementary data associated with this article can be found, in the online version, at http://dx.doi.org/10.1016/j.poly.2015.10.026.

References

[1] J. Chen, J. Stubbe, Nat. Rev. Cancer 5 (2005) 102.
[2] H. Umezawa, Prog. Biochem. Pharmacol. 11 (1976) 18.
[3] R.P. Hertzberg, P.B. Dervan, J. Am. Chem. Soc. 104 (1982) 313.
[4] T.A. Berg, B.L. Feringa, G. Roelfes, Chem. Commun. (2007) 180.
[5] A. Mukherjee, S. Dhar, M. Nethaji, A.R. Chakravarty, Dalton Trans. (2005) 349.
[6] E.L.M. Wong, G.S. Fang, C.M. Che, N. Zhu, Chem. Commun. (2005) 4578.
[7] D.Y. Dawson, S.E. Hudson, P.K. Mascharak, J. Inorg. Biochem. 47 (1992) 109.
[8] M. Otsuka, T. Masuda, A. Haupt, M. Ohno, T. Shiraki, Y. Sugiura, K. Maeda, J. Am. Chem. Soc. 112 (1990) 838.
[9] R.M. Burger, Chem. Rev. 98 (1998) 1153.
[10] U. Basu, I. Khan, A. Hussain, P. Kondaiah, A.R. Chakravarty, Angew. Chem., Int. Ed. 51 (2012) 2658.

[11] U. Basu, I. Pant, A. Hussain, P. Kondaiah, A.R. Chakravarty, Inorg. Chem. 54 (2015) 3748.
[12] A. Garai, U. Basu, I. Khan, I. Pant, A. Hussain, P. Kondaiah, A.R. Chakravarty, Polyhedron 73 (2014) 124.
[13] U. Basu, I. Khan, A. Hussain, B. Gole, P. Kondaiah, A.R. Chakravarty, Inorg. Chem. 53 (2014) 2152.
[14] A. Garai, U. Basu, I. Pant, P. Kondaiah, A.R. Chakravarty, J. Chem. Sci. 127 (2015) 609.
[15] M. Roy, S. Saha, A.K. Patra, M. Nethaji, A.R. Chakravarty, Inorg. Chem 46 (2007) 4368.
[16] F.S. Mackay, J.A. Woods, P. Heringová, J. Kašpárková, A.M. Pizarro, S.A. Moggach, S. Parsons, V. Brabec, P.J. Sadler, Proc. Nat. Acad. Sci. USA 104 (2007) 20743.
[17] N.L. Fry, P.K. Mascharak, Acc. Chem. Res. 44 (2011) 289.
[18] H.T. Chifotides, K.R. Dunbar, Acc. Chem. Res. 38 (2005) 146.
[19] (a) S. Banerjee, A. Dixit, R.N. Shridharan, A.A. Karande, A.R. Chakravarty, Chem. Commun. 50 (2014) 5590;
(b) S. Banerjee, A. Hussain, P. Prasad, I. Khan, B. Banik, P. Kondaiah, A.R. Chakravarty, Eur. J. Inorg. Chem. (2012) 3899.
[20] S. Banerjee, A. Dixit, A.A. Karande, A.R. Chakravarty, Eur. J. Inorg. Chem. (2015) 447.
[21] T.K. Goswami, B.V.S.K. Chakravarthi, M. Roy, A.A. Karande, A.R. Chakravarty, Inorg. Chem. 50 (2011) 8452.
[22] A. Bhattacharyya, A. Dixit, K. Mitra, S. Banerjee, A.A. Karande, A.R. Chakravarty, Med. Chem. Commun. 6 (2015) 846.
[23] R. Bonnett, Chemical Aspects of Photodynamic Therapy, Gordon & Breach, London, UK, 2000.
[24] J.F. Lovell, T.W.B. Liu, J. Chen, G. Zheng, Chem. Rev. 110 (2010) 2839.
[25] J.P. Celli, B.Q. Spring, I. Rizvi, C.L. Evans, K.S. Samkoe, S. Verma, B.W. Pogue, T. Hasan, Chem. Rev. 110 (2010) 2795.
[26] (a) N.A. Smith, P.J. Sadler, Phil. Trans. Royal Soc. A 371 (2013) 20120519;
(b) S. Banerjee, A.R. Chakravarty, Acc. Chem. Res. 48 (2015) 2075.
[27] U. Schatzschneider, Eur. J. Inorg. Chem. (2010) 1451.
[28] G. Cair, G. Cairo, F. Bernuzzi, S. Recalcati, Genes Nutr. 1 (2006) 25.
[29] J.L. Heath, J.M. Weiss, C.P. Lavau, D.S. Wechsler, Nutrients 5 (2013) 2836.
[30] J. Hay, S. Shahzeidi, G. Laurent, Arch. Toxicol. 65 (1991) 81.
[31] D. Rojas, A.M. García, A. Vega, Y. Moreno, D. Venegas-Yazigi, M.T. Garland, J. Manzur, Inorg. Chem. 43 (2004) 6324.
[32] L.A. Mullice, R.H. Laye, L.P. Harding, N.J. Buurma, S.J.A. Pope, New J. Chem. 32 (2008) 2140.
[33] N. Walker, D. Stuart, Acta Crystallogr., Sect. A 39 (1983) 158.
[34] G.M. Sheldrick, SHELX-97, Programs for crystal structure solution and refinement, University of Göttingen, Göttingen, Germany, 1997.
[35] C.K. Johnson, ORTEP, Report ORNL-5138, Oak Ridge National Laboratory, Oak Ridge, TN, 1976.
[36] L. Zhang, W. Liu, K.K. Szumlinski, J. Lew, Proc. Natl. Acad. Sci. USA 109 (2012) 20041.
[37] T. Takanashi, Y. Ogura, H. Taguchi, M. Hashizoe, Y. Honda, Invest. Ophthalmol. Vis. Sci. 38 (1997) 2721.
[38] J.D. McGhee, P.H. Von Hippel, J. Mol. Biol. 86 (1974) 469.
[39] M.T. Carter, M. Rodriguez, A.J. Bard, J. Am. Chem. Soc. 111 (1989) 8901.
[40] T.A. Sherstneva, K.P. Birin, V.V. Arslanov, Prot. Met. 49 (2013) 72.
[41] K. Nakamoto, Infrared and Raman Spectra of Inorganic and Coordination Compounds, John Wiley & Sons, New York, 1997.
[42] A.W. Addison, S. Burman, C.G. Wahlgren, O.A. Rajan, T.M. Rowe, E. Sinn, J. Chem. Soc. Dalton Trans. (1987) 2621.
[43] E. Delaey, F. van Laar, D. De Vos, A. Kamuhabwa, P. Jacobs, P. de Witte, J. Photochem. Photobiol. B 55 (2000) 27.